

# Simulation of Fermionic circuits using Majorana Propagation

Aaron Miller,<sup>1</sup> Zoë Holmes,<sup>1</sup> Özlem Salehi,<sup>1</sup> Rahul Chakraborty,<sup>1</sup> Anton Nykänen,<sup>1</sup> Zoltán Zimborás,<sup>1</sup> Adam Glos,<sup>1</sup> and Guillermo García-Pérez<sup>1,\*</sup>

<sup>1</sup>*Algorithmiq Ltd, Kanavakatu 3 C, FI-00160 Helsinki, Finland*

(Dated: April 1, 2025)

We introduce Majorana Propagation, an algorithmic framework for the classical simulation of Fermionic circuits. Inspired by Pauli Propagation, Majorana Propagation operates by applying successive truncations throughout the Heisenberg evolution of the observable. We identify *monomial length* as an effective truncation strategy for typical, unstructured circuits by proving that high-length Majorana monomials are exponentially unlikely to contribute to expectation values and the backflow of high-length monomials to lower-length monomials is quadratically suppressed. Majorana Propagation can be used either independently, or in conjunction with quantum hardware, to simulate Fermionic systems relevant to quantum chemistry and condensed matter. We exemplify this by using Majorana Propagation to find circuits that approximate ground states for strongly correlated systems of up to 52 Fermionic modes. Our results indicate that Majorana Propagation is orders of magnitude faster and more accurate than state-of-the-art tensor-network-based circuit simulators.

## I. INTRODUCTION

Simulating many-body quantum systems is computationally challenging, despite its fundamental importance across various fields, including condensed-matter physics and quantum chemistry. Quantum computing offers new perspectives, powered by processors that exhibit quantum phenomena and are therefore not limited by them. Yet, operating quantum devices for practical purposes can benefit enormously from accurate classical circuit simulation algorithms [1]. These can be used, among other things, to produce good reference states for quantum simulation tasks, offloading costly circuit optimization routines to a classical machine.

In this context, Pauli Propagation (PP) has recently emerged as a new promising method for spin systems [2–15]. By leveraging typical features in the dynamics of Pauli strings evolving through a circuit, PP disregards terms that are expected to have a negligible contribution to the expectation value one is simulating, resulting in guaranteed accuracy for almost all circuits within a vast class. PP thus presents itself as a very natural way to simulate expectation values of spin circuits. Despite its recent conception, PP can already compete with well-established methods, such as tensor networks and neural network states. Furthermore, it allows for fast circuit optimization in variational scenarios thanks to surrogate simulation [6], and can be readily interfaced with quantum hardware [12, 15], as it operates at the circuit level.

However, the applicability of PP to other many-body systems, such as Fermionic ones, remains an open question. In particular, many quantum systems are mathematically described by algebras that do not have an equivalent to Pauli weight locality, a quantity central to PP. While these systems are mappable to qubit space, the

resulting Pauli operators are typically highly non-local, severely limiting the practicality of PP.

Here we present Majorana Propagation (MP), a PP-inspired classical simulation algorithm that can be naturally used for Fermionic systems. Differently from PP, MP does not operate at the level of Pauli weight; in fact, it does not even assume the decomposability of the algebra describing the system into tensor products of sub-system operators. Instead, MP leverages the typical behaviour of monomials spanning operator bases. Crucially, the Fermionic basis is effectively built ‘on the fly’ and so is not restricted to simulating free Fermion models but rather can be used to simulate systems living in exponentially large Lie algebras. Moreover, unlike tensor network methods or near-Clifford methods, our approach is not intrinsically targeting low entanglement or magic growth scenarios

A particularly promising application of MP is for optimizing circuits to prepare approximate ground states. Established quantum algorithms for energetic structure calculations, including near-term [16–25] and fault-tolerant [26–36] approaches, need to be initialized with good reference states, as their performance depends on the overlap between the reference and the ground state. How to find these remains an open question [37, 38], and heuristic variational ground state approximation methods are likely to play an important role.

Many of the most successful variational methods for ansatz generation construct Fermionic circuits that are then appropriately mapped to qubit space for hardware execution [39–45]. Operating in Fermion space has proved numerous advantages, including the facilitation of imposing known symmetries of the simulated system. However, historically, many of these methods also rely on the quantum device itself to carry out the optimization, which results in costly and unreliable feedback loops between a classical and a quantum computer [38, 46–50]. Here we show that MP can be used to classically simulate and optimize adaptive Fermionic circuit ansätze to

\* guille@algorithmiq.fi

find circuits for preparing approximate ground states of strongly correlated molecules [51].

Beyond ground states, MP may find use both as a stand-alone classical algorithm, and as a tool to be used in conjunction with quantum hardware, to study Fermionic systems. Potential applications range from simulating the dynamics of Fermionic systems [12, 15] to tackling classification problems with quantum data [50, 52].

## II. BACKGROUND

An  $N$ -mode Fermionic system in second quantization can be described in terms of  $N$  creation operators  $\{a_i^\dagger\}_{i=1}^N$  and annihilation operators  $\{a_i\}_{i=1}^N$  that satisfy the canonical anticommutation relations  $\{a_i, a_j\} = \{a_i^\dagger, a_j^\dagger\} = 0$ , and  $\{a_i^\dagger, a_j\} = \delta_{ij}$ . These operators act on the Fermionic Fock space  $\mathcal{F}(\mathbb{C}^N) \cong \bigoplus_{k=0}^N \wedge^k \mathbb{C}^N$ , which is a  $2^N$ -dimensional Hilbert space spanned by the so-called Fock basis. In this space, the Fermionic vacuum  $|\text{vac}_f\rangle$  the unique vector such that  $a_j |\text{vac}_f\rangle = 0$  for all  $j = 1, \dots, N$ . The remaining Fock basis elements can be constructed by considering all possible combinations of occupation numbers  $n_j \in \{0, 1\}$  as  $|n_1 n_2 \dots n_N\rangle := \prod_{j=1}^N (a_j^\dagger)^{n_j} |\text{vac}_f\rangle$ .

It is also common to define the Fermionic space with so-called Majorana operators  $\{m_k\}_{k=1}^{2N}$  as  $m_{2j-1} := a_j^\dagger + a_j$  and  $m_{2j} := i(a_j^\dagger - a_j)$ . Such operators obey many convenient properties, such as being unitary and self-adjoint, and satisfy simpler anti-commutation relations:

$$m_i^\dagger = m_i, \quad \{m_i, m_j\} = 2\delta_{ij}. \quad (1)$$

These  $2N$  Majorana operators are algebraically independent, that is, no two distinct products of them (ordered according to the indices) result in the same operator. Hence, up to a sign, each unique product of Majorana operators can be associated with a  $2N$ -dimensional binary vector  $\mathbf{b} = (b_1, \dots, b_{2N})$ ,  $b_i \in \{0, 1\}$  through the expression

$$M_{\mathbf{b}} = i^{r_{\mathbf{b}}} m_1^{b_1} m_2^{b_2} \dots m_{2N}^{b_{2N}}. \quad (2)$$

The imaginary unit  $i$  is included to ensure that  $M_{\mathbf{b}}$  is Hermitian<sup>1</sup>. The  $4^N$  operators  $\{M_{\mathbf{b}}\}_{\mathbf{b}}$  form a basis of the space of linear operators in the Hilbert space, thus any operator can be uniquely decomposed as a linear combination of them. We will refer to these operators as *Majorana monomials*. The length of a Majorana monomial,

defined as the 1-norm of vector  $\mathbf{b}$ ,  $\|\mathbf{b}\|_1 = \sum_{i=1}^{2N} b_i$ , will play a crucial role in this work. We will use the shorthand  $w$ -monomial to refer to length- $w$  Majorana monomials.

Majorana monomials share some algebraic similarities with Pauli strings: They are traceless (except for the length-0 monomial, i.e., the identity operator). Any two of them either commute or anti-commute, and they square up to identity  $M_{\mathbf{b}}^2 = \mathbb{I}$ . However, unlike Pauli strings, they are not decomposable as a tensor product of  $N$  single-mode operators, as Majorana operators are non-local. In fact, under fermion-to-qubit transformations, Majorana monomials are generally mapped to non-local Pauli strings [39], with Pauli weights spanning a wide range, even for fixed Majorana monomial length. This hinders the implementation of PP for Fermionic systems, as Pauli weight does not capture typical operator dynamics.

## III. MAJORANA MONOMIAL PROPAGATION

We consider the task of simulating expectation values of observables. That is, we want to compute

$$\langle H \rangle_{\boldsymbol{\theta}} = \text{Tr} [U(\boldsymbol{\theta}) \varrho U(\boldsymbol{\theta})^\dagger H] \quad (3)$$

given a unitary Fermionic circuit  $U(\boldsymbol{\theta})$ , an initial state  $\varrho$ , and an observable  $H$ . The initial state is typically a Fock basis state,  $\varrho = |n_1 n_2 \dots n_N\rangle \langle n_1 n_2 \dots n_N|$ . We further suppose the Fermionic circuit,

$$U(\boldsymbol{\theta}) = \prod_{j=1}^L e^{-i\theta_j M_{\mathbf{b}_j}/2}, \quad (4)$$

consists of a sequence of  $L$  Fermionic gates where each gate is generated by a Majorana monomial generator  $M_{\mathbf{b}_j}$  and the  $\theta_j$  are real parameters. Finally we assume that the observable  $H$  has a known expansion into Majorana monomials  $H = \sum_{\mathbf{b}} \alpha_{\mathbf{b}} M_{\mathbf{b}}$ . Observables  $H$  of physical interest are spanned by Majorana monomials of low, even length. For instance, most Hamiltonians in quantum chemistry and materials contain only length-2 and length-4 terms and thus the number of terms in the expansion will typically scale at worst polynomially in  $N$ .

Our proposed Majorana Propagation algorithm, schematically depicted in Fig. 1, works naturally in the Heisenberg picture. We take each monomial in the expansion of  $H$  and back-propagate it under each of the gates in the circuit. The evolution of monomials under Fermionic gates takes a conveniently compact form. Namely, in direct analogy with the Pauli case, if the propagated monomial  $M_{\mathbf{b}}$  commutes with the generator of rotation  $M_{\mathbf{b}_j}$  then the monomial is left unchanged but otherwise it branches into the sum of two monomials with a cosine or sine coefficient depending on the rotation angles:

$$M_{\mathbf{b}} \xrightarrow{e^{-i\theta_j M_{\mathbf{b}_j}/2}} \cos(\theta_j) M_{\mathbf{b}} + \sin(\theta_j) i M_{\mathbf{b}_j} M_{\mathbf{b}}. \quad (5)$$

<sup>1</sup> The  $i$  is necessary whenever inverting the product sequence involves an odd number of permutations. That is, the value of  $r_{\mathbf{b}}$  depends on the length  $w = \|\mathbf{b}\|_1$  of the monomial. As shown in Appendix A, if either  $w$  or  $w - 1$  is a multiple of 4,  $r = 0$ . Otherwise,  $r = 1$ .

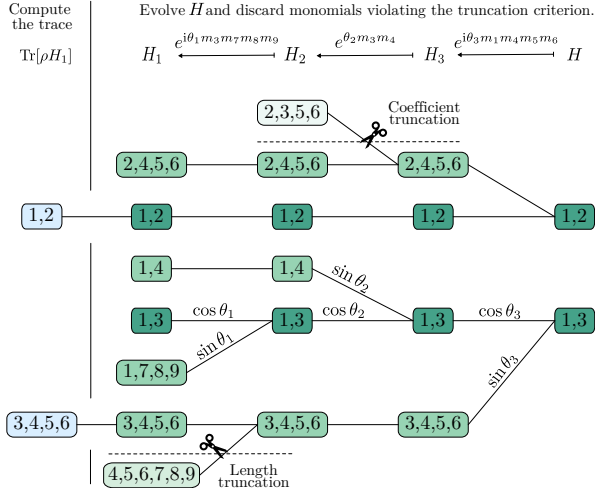


Figure 1. **Illustration of Majorana Propagation.** The observable  $H$  is spanned by two length-2 terms,  $im_1m_2$  and  $im_1m_3$ . The first gate, generated by  $m_1m_4m_5m_6$  anti-commutes with both terms, leading to branching into higher length monomials. The intensity of the colour represents the coefficient accompanying each monomial. Assuming small angles, the sine branches are paler than their precursors. The figure further depicts two different truncation events, one where a length-4 monomial is eliminated because of its coefficient reaching a very low value, and a second one where a length-6 monomial exceeds the length threshold  $w^* = 4$ . In the final computation of the trace, only two of the surviving monomials are paired and thus contribute to the estimate.

Applying Eq. (5) iteratively on each of the gates in Eq. (4), starting with the rotation under  $M_{b_L}$ , we end up with a new sum of Majorana monomials  $\sum_b c_b(\theta) M_b$  where  $c_b(\theta)$  are the coefficients of the back-propagated monomials  $M_b$ . These coefficients capture both the initial length of each of the relevant monomial in the target observable  $H$  and the sine and cosine coefficients that have been picked up during the propagation. Finally, we compute the overlap of these monomials with the initial state  $\rho$  to compute the expectation value as

$$f(\theta) = \sum_j c_b(\theta) \text{Tr}[\rho M_b]. \quad (6)$$

If the rotation angles for the circuit one wishes to simulate are known in advance then the sine and cosine terms take numerical values and the  $c_b(\theta)$  coefficients can be stored numerically. However, if the values of  $\theta$  are not known in advance, or one is interested in computing the expectation value in Eq. (3) for a wide range of  $\theta$  values, one can instead symbolically represent the coefficients  $c_b(\theta)$ . Such *surrogate* models have a substantial time and memory overhead, but after this pre-processing step, enable rapid re-evaluation of the expectation value [6, 8, 12].

While we here focus on unitary Fermionic circuits that have been compiled into products of monomial rotations, as per Eq. (4), we stress that Majorana Propagation can

be applied more generally to compute expectation values for circuits composed of a sequence of  $L$  linear maps  $\mathcal{C} = C_L \circ \dots \circ C_1$ . In that case, one simply computes an analogous expression to Eq. (5) for the action of each  $C_j$  on an arbitrary Majorana monomial.

In its raw form, the number of monomials in the final expression for the expectation value, Eq. (6), will blow up exponentially with the number of gates in the circuit that induce a splitting. We therefore employ *truncation* schemes to drastically reduce the computational resources. There are two main families of truncations that can be employed to make the simulation more efficient, namely 1) ones that truncate small (or likely small) coefficients  $c_b$  and 2) ones that truncate any monomial  $M_b$  where  $\text{Tr}[\rho M_b]$  is small (or likely small). Inevitably these truncations will reduce the accuracy of the simulation but in many cases, the reduction in accuracy can be kept small.

If we are simulating a circuit with fixed angles, i.e., the  $\theta$  parameter for the circuit is already known, then the simplest truncation strategy is *coefficient truncation*. That is, we can keep track of the coefficients in front of each monomial as we back-propagate each term through the circuit and simply truncate (drop) any terms that have an absolute value below some predefined value.

Alternatively, in the case of *surrogate* simulation where the angles  $\theta$  are not known in advance, if one is primarily interested in simulating within some small angle range (e.g., in the case of simulating Trotterization-like circuits) one can use the so-called *small angle* truncation scheme [5, 12]. Namely, we can leverage the fact that when  $\theta$  are small then sine contributions to the coefficients  $c_b$  in Eq. (6) are much smaller than cosine contributions. Thus we can prune paths with many sine coefficients without substantially changing the estimation of the expectation value (see Fig. 1). In Appendix B we provide theoretical guarantees for this approach that follow directly from the analogous findings for Pauli Propagation presented in Ref. [12].

The second truncation strategy, whereby one aims to cut terms from the sum in Eq. (6) where  $\text{Tr}[\rho M_b]$  is likely small, is more subtle. While potentially there are a number of different strategies one could take here, we will make use of the observation that in order for a term  $\text{Tr}[\rho M_b]$  to be non-zero all the Majorana operators in the monomial  $M_b$  are *paired*. That is,  $\text{Tr}[\rho M_b] \neq 0$  if and only if for every even Majorana operator  $m_{2i}$  in the Majorana operator  $m_{2i+1}$  is also in the monomial (this can be seen immediately from the definition of the Majorana operator, Eq. (A3), and noting that  $\langle \phi | a_i | \phi \rangle = \langle \phi | a_i^\dagger | \phi \rangle = 0$  for any Fock basis state  $|\phi\rangle$ ). Next we observe that in general the higher the length  $w$  of the Majorana monomial (for  $w < N$ ) the lower the probability that the monomial is paired. This motivates a *length truncation* strategy. At each step, after each gate is applied, all terms corresponding to Majorana monomials with length above a certain threshold are to be discarded. This idea is de-

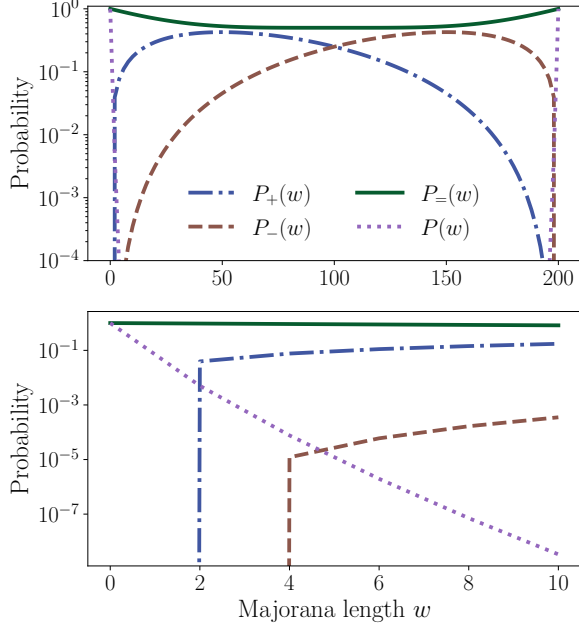


Figure 2. **Suppression of high-length modes and back-flow.** Transition and pairing probabilities for  $N = 100$  modes and a randomly chosen length-4 gate for all  $w$  lengths from 0 to  $2N$  (top) and for  $w \leq 10$  (bottom). For small  $w$ ,  $P_+$  is substantially larger than  $P_-$ , which tends to drive monomial length upwards in the event of branching. The roles of  $P_+$  and  $P_-$  are symmetrically inverted at  $w = N$ , so successive branching tends to trap Majorana monomials around that point. The highest probability corresponds to no-branching events,  $P_+ = 1 - [P_+ + P_-]$ . At the end of the Heisenberg evolution, monomials are traced with a Fock basis state. The probability for a length- $w$  monomial to contribute to the trace,  $P(w)$ , decreases very rapidly in  $w$ , rendering the contribution of high- $w$  terms irrelevant.

picted in Fig. 1 and analyzed in more detail in the next section.

#### IV. LENGTH TRUNCATION

In order to study Majorana length truncation analytically, we will consider unstructured Fermionic circuits with gates generated by Majorana monomials with  $\|\mathbf{b}_j\|_1$  an even number smaller than or equal to some  $k^* \ll N$ . Unstructured here means that the generators are randomly sampled from the pool of such operators,  $\{\mathbf{M}_{\mathbf{b}} : \|\mathbf{b}\|_1 \leq k^*, \|\mathbf{b}\|_1 \bmod 2 = 0\}$ . This class of circuits can be regarded as a mathematically tractable, oversimplified model of certain relevant circuits, such as iteratively constructed variational circuits [51], which should suffice to elucidate the basic phenomena at play in Majorana Propagation for typical Fermionic circuits.

The first important point motivating Majorana length truncation is the fact that most high-length terms do not contribute to the expectation value  $\langle H \rangle$ . As discussed

above, only paired Majorana monomials yield non-zero values when traced with a Fock basis state. The probability  $P(w)$  for a randomly chosen  $w$ -monomial to be paired, is given by

$$P(w) = \frac{\binom{N}{w/2}}{\binom{2N}{w}} \quad (7)$$

and as depicted in Fig. 2, is very small unless  $w$  is close to 0 or to  $2N$ . This is stated more precisely in the following theorem (see Appendix C 1 for proof).

**Theorem 1** (The contribution of high length Majorana monomials are exponentially suppressed). *The probability  $P(w)$  that any randomly chosen  $N$ -mode Majorana monomial with length  $w$ , where both  $w \in \Theta(N)$  and  $(2N - w) \in \Theta(N)$ , has a non-zero expectation in any given Fock state is exponentially suppressed in  $N$ , that is*

$$P(w) \in \mathcal{O}(r^{-N}), \quad (8)$$

where  $r > 1$ . Furthermore, the minimal probability is obtained for  $w = N$  with

$$\min_w P(w) = P(N) \in \mathcal{O}(2^{-N}). \quad (9)$$

Conversely, if  $w \in \mathcal{O}(1)$  we have that

$$P(w) \in \Omega\left(\frac{1}{\text{poly}(N)}\right). \quad (10)$$

While crucial, this fact alone does not justify Majorana length truncation. Truncating below a certain threshold  $w^* \ll N$  disposes of terms with length  $w \approx 2N$ , if any, which can potentially contribute non-negligibly to the expectation value. Furthermore, the fact that these Majorana monomials do not contribute significantly to the trace with a Fock basis state at best justifies the truncation at the very end of the evolution, once all gates have been applied. At intermediate steps, high-length Majorana monomials could flow back into the low-length subspace, so eliminating them along the way could introduce significant errors. To understand why these events are typically very unlikely, we must turn our attention to the analysis of typical Majorana monomial dynamics.

From the algebraic properties of Majorana operators, Eq. (1), it can be seen that the two monomials anticommute if and only if they have an odd number of Majorana operators in common, that is, iff the number of overlapping operators  $s$ , which can be computed as  $s = \mathbf{b} \cdot \mathbf{b}_j$ , is odd. We can draw several interesting conclusions from this fact.

First, let  $k := \|\mathbf{b}_j\|_1$  and  $w := \|\mathbf{b}\|_1$ . As a consequence of the properties in Eq. (1), more precisely of the fact that even repetitions of Majorana operators in any product cancel out, the length  $w'$  of the monomial in the sine branch,  $i\mathbf{M}_{\mathbf{b}_j}\mathbf{M}_{\mathbf{b}}$ , is the sum of the lengths of the two original monomials,  $w + k$ , minus twice their overlap,  $s$ :

$$w' = w + k - 2s. \quad (11)$$

Hence, even- $k$  gates preserve Majorana length parity; in physically relevant scenarios, where all gate generators and monomials in the observable are even, one only needs to consider the even-monomial subspace.

Second, for gates generated by so-called single-excitation, or one-body monomials ( $k = 2$ ), branching can only occur for  $s = 1$ , and so  $w' = w$ . In other words, these gates preserve Majorana length and can therefore be accounted for exactly by the algorithm: no additional truncations are required in order to restrict the operator to the subspace.

Third, according to Eq. (11), the length  $w'$  of the new monomial in the sine branch is  $w' > w$  if  $s < k/2$ ,  $w' < w$  if  $s > k/2$ , and  $w' = w$  if  $s = k/2$ . Importantly, for  $w, k \ll N$ , smaller values of  $s$  are much more likely than larger ones. This can be seen intuitively: drawing  $k$  distinct Majorana operators out of the set of all  $2N$ , the most likely event is for none of them to match those within the  $w$  operators in  $M_b$ . Consequently, there is an asymmetry in the dynamics whereby branching events tend to increase Majorana length with higher likelihood than they tend to decrease it, preventing backflows of monomials back into the low-length subspace. Crucially, for  $w > N$ , the effect is reversed and the dynamics tends to decrease Majorana length, so the dynamics tends to cluster monomials around  $w = N$ .

This can be seen more formally, since the probability for the overlap to be exactly  $s$  can be derived analytically,

$$P(N, w, k, s) = \frac{\binom{k}{s} \binom{2N-k}{w-s}}{\binom{2N}{w}}, \quad (12)$$

from which the probabilities for the length to increase or decrease,  $P_+$  and  $P_-$ , can be computed by simply summing over  $s$  for  $s < k/2$  and  $s > k/2$ , respectively. These quantities are illustrated in Fig. 2. We note the invariance of Eq. (12) with respect to  $w \rightarrow 2N - w$ ,  $s \rightarrow k - s$ , which explains the reversal of the phenomenon for  $w > N$ . Finally, using these expressions, it is possible to analyze the behaviour of the ratio  $R := P_-/P_+$ , which quantifies the asymmetry in the dynamics and to show that, for fixed  $w$  and  $k$ , it vanishes quadratically in  $N$ , making backflows increasingly unlikely as  $N$  increases. All these points are captured formally in the following theorem (proof in Appendix C2).

**Theorem 2** (Suppression of backflow). *Consider the propagation of a length  $w$  Majorana monomial  $M$  under a length  $k$  generator of rotation  $M'$  as per Eq. (5). We assume that  $[M', M] \neq 0$  such that the propagation causes branching and we denote the length of the new Majorana monomial,  $M'M$ , as  $w'$ . Let  $P_+$  and  $P_-$  denote the probabilities that the propagation increases ( $w' > w$ ) and decreases ( $w < w'$ ) operator length. The following statements hold:*

1. Any rotation under a  $k = 2$  length generator  $M$  leaves length  $w$  unchanged,  $P_+ = P_- = 0$ .

2. For any  $w \in \mathcal{O}(1)$  and  $k \in \mathcal{O}(1)$  with  $2 \leq k \leq w$  such that  $wk < N$  we have that

$$R := P_-/P_+ \in \mathcal{O}(1/N^2). \quad (13)$$

This analysis paints a very clear picture of Majorana monomial dynamics for typical circuits in the Heisenberg picture: as the operator evolves through the gates in the circuit, operator branching leads to ever-increasing Majorana length, with very low likelihood of length-decreasing events, until length  $w \approx N$  is reached. After that point, branching tends to decrease length, trapping monomials around  $w = N$ .

The algorithm introduced in this work takes advantage of this dynamics. As explained above, the monomials clustering around  $w = N$  contribute exponentially little to the trace with the Fock basis state, so they can be neglected. Due to the inversion in the branching imbalance for  $w > N$ , the terms with  $w \approx 2N$  are never populated, so they need not be considered in the simulation. Moreover, since backflow probability throughout the dynamics is very small, there is no need to account for high-length monomials until they reach the  $w \approx N$  regime. Hence, they can be neglected early on, as soon as they leave the low-length subspace.

## V. IMPLEMENTATION

We now test Majorana Propagation in the context of variational circuits for quantum chemistry. Given an input Hamiltonian  $H$ , the goal is to find a circuit approximating its ground state to a certain degree. The accuracy of the approximation varies depending on the specific application at hand, but one is typically interested in obtaining non-negligible overlaps with the ground state.

Within the plethora of variational optimization methods for chemistry, adaptive methods have proved to be particularly gate efficient, finding good reference states with relatively modest gate complexity. Here we will explore a classical algorithm inspired by ADAPT-VQE [51, 53–56], where gates are sequentially selected from a Majoranic pool and added to the circuit as to minimize the energy of the output state. The operators in the pool are generally low-body, that is, spanned by low-length Majorana monomials. This adaptive ansatz construction strategy typically results in rather irregular circuits with gates generated by low-length monomials—circuits for which the unstructured circuit class introduced above should be a reasonable model.

The Hamiltonians considered in this section model the electronic structure of the TLD1433 molecule, a ruthenium-based photosensitizer currently undergoing clinical trials for non-muscle invasive bladder cancer [57], with different active sizes comprising  $N = \{28, 40, 52\}$  modes. This is a strongly correlated system which state-of-the-art classical methods, such as DMRG, struggle to solve for larger active spaces. In our simulations, we use

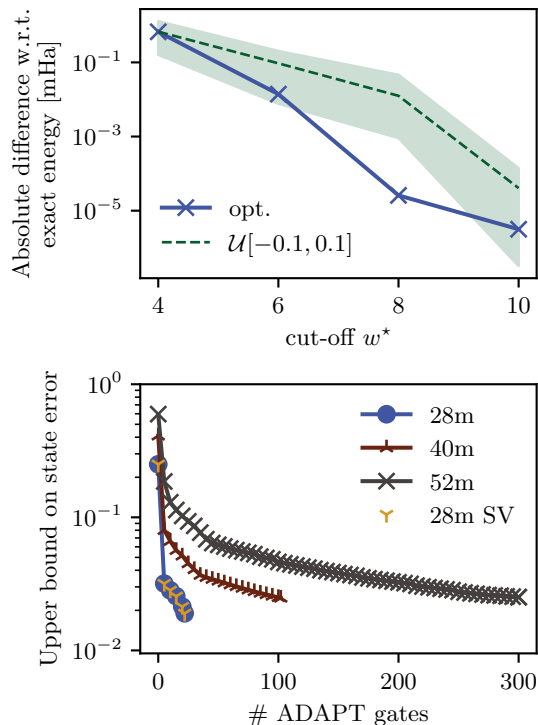


Figure 3. **Majorana Propagation implementation for ground states.** Top: The blue curve depicts the error in the estimated energy as a function of monomial length cut-off  $w^*$  for a 28-mode MP-simulated ADAPT-VQE circuit containing 22 Fermionic gates, computed by comparison against statevector simulation (SV). The error of the MP simulation decreases exponentially from below chemical precision (1.6 mHa) for  $w^* = 4$  to around numerical precision for  $w^* = 10$ . The green curve shows the same quantity for 5 circuits obtained by uniformly randomizing angles in the range  $[-0.1, 0.1]$ . The shaded area indicates the maximal and minimal errors attained. Bottom: The ADAPT-VQE inspired algorithm is run classically using MP to simulate the circuits for increasing problem sizes (solid lines). The  $x$ -axis reflects the number of Fermionic gates in the circuit. The  $y$ -axis value is the error in the energy, computed with MP with  $w^* = 6$ , divided by the spectral gap of the Hamiltonian, which bounds the lack of overlap with the ground state. For 28 modes we verify the accuracy of the MP simulation by computing the equivalent error via a SV simulation (yellow markers). SV simulation for the larger problems was not tractable. Only every 5th marker is included to improve readability.

a slightly refined monomial-length-based truncation criterion that will be explained in detail in a forthcoming version of this manuscript.

In Fig. 3 (top), we plot the error in the energy estimated with MP as a function of the length cut-off  $w^*$  for an ADAPT-VQE circuit comprising 22 Fermionic gates—equivalent to a 616-CNOT circuit on all-to-all connectivity (see Appendix D)—optimized for the 28-mode active space Hamiltonian. The error  $\varepsilon$  is computed as  $\varepsilon = |E_{\text{MP}}(w^*) - E_{\text{sv}}|$ , where  $E_{\text{sv}}$  is the exact energy (up

Number of modes	Majorana pre-pro.	Propagation estim.	Qiskit SV	CUDA-Q SV	CUDA-Q MPS
28	0.32 s	0.0023 s	3.71 h	12.18 min	32.15 min
40	7.86 s	0.0461 s	—	—	10.10 h
52	104.93 s	0.2145 s	—	—	> 24 h

Table I. **Comparison of simulation times.** Here we compare the times to estimate the energy of the TLD1433 Hamiltonians (of various active space sizes) for an approximate ground state for various simulation methods. The approximate ground states have been found by optimizing our ADAPT-VQE inspired ansatz with MP to within 10 mHa error with respect to the DMRG energy benchmark. The two columns for MP refer to the pre-processing time for a given ansatz (i.e., the time to build the surrogate) and to the subsequent energy estimation time (i.e., the time to evaluate the surrogate), respectively. Any additional estimations of the energy for different circuit parameters  $\theta$  only incur a time given in the second column. We note that for 28 qubits, MP approximates the energy within an absolute error of  $\approx 1.39 \cdot 10^{-2}$  mHa with respect to the CUDA-Q statevector exact result, while CUDA-Q MPS method gives an approximation error of  $\approx 2.71$  mHa.

to numerical precision) obtained via statevector simulation. Remarkably, even for  $w^* = 4$ , MP produces an estimate with an error below chemical precision (1.6 mHa), with the error decreasing approximately exponentially as a function of the cut-off to nearly numerical precision for  $w^* = 10$ . A similar behaviour is observed when the angles are randomized within the parameter range in the optimized circuit, although the decay in  $w^*$  is slower.

For the larger active space sizes, statevector simulations are out of reach, which makes benchmarking MP challenging. However, we can take advantage of the fact that we are using MP in the context of ground state chemistry. State-of-the-art computational chemistry methods, like DMRG, can produce very accurate estimates of the ground state energy for the considered system sizes. We can therefore compare the energy obtained by training ADAPT-VQE circuits with MP against these benchmarks to indirectly test our simulator. A well-behaved convergence towards the benchmark ground state energy is an implicit signature of MP’s simulation accuracy.

In many applications, the relevant figure of merit quantifying the quality of a reference state  $|\phi\rangle$  is its overlap with the ground state  $|\langle\phi|\psi_0\rangle|$ . Given the error in the energy,  $|E - E_0|$ , the overlap can be lower-bounded if the spectral gap of the Hamiltonian is known (see Appendix E). Thus, using the spectral gap computed with DMRG, we can upper-bound the *state error*, which we define as  $1 - |\langle\phi|\psi_0\rangle|$ . The bottom plot in Fig. 3 shows the upper bound to the state error as a function of the number of Fermionic gates in the circuit as the adaptive training progresses. All cases show a rapid convergence, reaching an overlap of at least 97% with the ground state with 22, 102, and 300 Fermionic gates for



the three active space sizes (the simulations were manually interrupted upon reaching a absolute error of 10 mHa). When mapped to qubit space and transpiled for an all-to-all connectivity quantum computer, the equivalent circuits contain 616, 3470, and 13,676 CNOTs, respectively, which highlights the complexity of the obtained states.

As explained above, these results provide an indirect validation of the approach. In Fig. 3 (bottom), two sources of error are compounded: the error of the circuit itself, and the estimation error incurred by MP. Thus, it is in principle possible for the estimation error to contribute as to lower the energy, resulting in estimated energies closer to the ground state than the true circuits'. In order to assess to what extent this is the case, we evaluate the energy of several intermediate circuits obtained throughout the 28-mode ADAPT-VQE simulation with statevector. As shown in the figure, the state error bounds computed with MP and statevector agree almost perfectly. This shows that MP is accurate enough to support the successful classical simulation of ADAPT-VQE circuits, leading to a collection of circuits increasingly converging to the ground state.

Finally, Table I reports run-time benchmarks for energy estimation with MP and other methods: two statevector simulators (Qiskit and CUDA-Q), as well as CUDA-Q MPS simulator, a tensor network-based circuit simulator. The circuits used are the converged ADAPT-VQE circuits from Fig. 3 (bottom), transpiled to qubit space, resulting in the CNOT counts reported above. While statevector simulators are exact (up to numerical precision), they scale exponentially. Thus, only the 28-mode circuit could be simulated with these simulators with reasonable resources. MP and CUDA-Q MPS, on the other hand, produce approximate estimates but run in polynomial time. Details on the implementation of these methods can be found in Appendix D. Interestingly, in addition to simulating these circuits considerably faster than CUDA-Q MPS, the 28-mode result is also nearly two orders of magnitude more accurate, approximating the statevector energy within  $\approx 1.39 \cdot 10^{-2}$  mHa, as opposed to the  $\approx 2.71$  mHa error in the MPS simulation.

Crucially, most of the time taken by the MP calculations is in a pre-processing stage, after which the re-evaluation of the energy for different parameter values  $\theta$  is very fast. This feature is particularly convenient for variational circuits, which benefits from parameter optimization.

## VI. DISCUSSION

Our analytical results portray MP as a very natural framework for the simulation of Fermionic circuits. While originally inspired by PP, MP is not equivalent to the former. MP leverages newly identified phenomena in the behaviour of basis monomials, which are not related to

Pauli weight. The underlying assumption in our analysis, namely that circuits are unstructured, with gate generators randomly chosen from a set of bounded-length monomials, seems particularly appropriate to model iteratively constructed ground state approximating circuits. Our analysis also sheds light on the working principles behind approaches like Majorana-length-damping in tensor network methods for Fermionic systems [58].

Our numerical results substantiate that MP can be used to classically simulate ADAPT-VQE to produce circuits with significant overlap with the ground state in strongly correlated systems. In our simulations, MP was able to outperform state-of-the-art, tensor network circuit simulators. It would be interesting to compare its performance to more recently proposed approximate simulation methods for Fermionic circuits, like Refs. [59–62]. Since MP does not rely on the sparsity of the wavefunction in the Fock basis, and since single-excitation gates do not require additional truncation in MP, MP may produce more accurate estimations for circuits with many such excitations leading to dense states. Similarly, we stress that MP is strictly more powerful and efficient than ‘gsim’ approaches [63–67] as the basis of the algebra is effectively generated ‘on the fly’ during the simulation (rather than in advance) and so is not restricted to free Fermionic models with polynomially scaling Lie algebras.

MP is, by design, well-suited to being interfaced with quantum hardware with the aid of Fermion-to-qubit mappings [39–43]. Through these transformations, the circuits obtained via MP can be readily executed on hardware. While MP can be used to efficiently approximate expectation values of observables, hardware execution will be needed in many contexts, even when sampling—a task MP cannot be used for—is not required. For instance, in many computational pipelines, it may generally prove more efficient to use MP to train a circuit up to a limited but sufficient level of accuracy and then use it as a reference for another algorithm, such as QPE, than solving the problem purely classically.

More generally, including contexts like dynamical simulations and machine learning and beyond, hybrid methods where the outputs of a quantum algorithm are further processed with the help of a classical MP simulation have the potential to make the most of size and depth-limited near-term quantum hardware by reducing the load on the quantum device. But even in the fault tolerant era such hybrid approaches will likely remain valuable and MP will prove useful for finding good initial states and processing the outputs of fermion simulations on quantum hardware.

*Acknowledgements* Work on “Quantum Computing for Photon-Drug Interactions in Cancer Prevention and Treatment” is supported by Wellcome Leap as part of the Q4Bio Program. We thank Pi A. B. Hasse, Stefan Knecht, Fabijan Pavosevic, Martina Stella, and Fabio Tarocco for providing the TLD1433 Hamiltonians and the corresponding DMRG benchmarks. We also thank

Ludmila A. S. Botelho and Roberto Di Remigio for their code optimization advice.

*Note* During the completion of this work, we became aware of independent work by Matteo D’Anna and Jannes Nys where they employ a related approach to study dynamics in Fermionic lattice models.

*Competing interests* Elements of this work are included in patent applications filed by Algorithmiq Oy currently pending with the European Patent Office.

*Author contributions* GGP conceived the method. AM implemented the method. ZH and GGP formalized the theory and wrote the first version of the manuscript. AM, OS, AN, RC, and AG implemented and executed the ADAPT-VQE simulations under AG’s direction. AM, OS, and AG produced the figures. All authors participated to discussions and to the writing of the manuscript.

- 
- [1] J. Preskill, Quantum computing in the NISQ era and beyond, *Quantum* **2**, 79 (2018).
  - [2] P. Rall, D. Liang, J. Cook, and W. Kretschmer, Simulation of qubit quantum circuits via pauli propagation, *Physical Review A* **99**, 062337 (2019).
  - [3] D. Aharonov, X. Gao, Z. Landau, Y. Liu, and U. Vazirani, A polynomial-time classical algorithm for noisy random circuit sampling, *Proceedings of the 55th Annual ACM Symposium on Theory of Computing*, 945 (2023).
  - [4] T. Rakovszky, C. Von Keyserlingk, and F. Pollmann, Dissipation-assisted operator evolution method for capturing hydrodynamic transport, *Physical Review B* **105**, 075131 (2022).
  - [5] T. Begušić, K. Hejazi, and G. K. Chan, Simulating quantum circuit expectation values by Clifford perturbation theory, arXiv preprint arXiv:2306.04797 (2023).
  - [6] E. Fontana, M. S. Rudolph, R. Duncan, I. Rungger, and C. Cirstoiu, Classical simulations of noisy variational quantum circuits, arXiv preprint arXiv:2306.05400 (2023).
  - [7] Y. Shao, F. Wei, S. Cheng, and Z. Liu, Simulating quantum mean values in noisy variational quantum algorithms: A polynomial-scale approach, arXiv preprint arXiv:2306.05804 (2023).
  - [8] M. S. Rudolph, E. Fontana, Z. Holmes, and L. Cincio, Classical surrogate simulation of quantum systems with LOWESA, arXiv preprint arXiv:2308.09109 (2023).
  - [9] T. Schuster, C. Yin, X. Gao, and N. Y. Yao, A polynomial-time classical algorithm for noisy quantum circuits, arXiv preprint arXiv:2407.12768 <https://doi.org/10.48550/arXiv.2407.12768> (2024).
  - [10] A. Angrisani, A. Schmidhuber, M. S. Rudolph, M. Cerezo, Z. Holmes, and H.-Y. Huang, Classically estimating observables of noiseless quantum circuits, arXiv preprint arXiv:2409.01706 (2024).
  - [11] G. González-García, J. I. Cirac, and R. Trivedi, Pauli path simulations of noisy quantum circuits beyond average case, arXiv preprint arXiv:2407.16068 (2024).
  - [12] S. Lerch, R. Puig, M. Rudolph, A. Angrisani, T. Jones, M. Cerezo, S. Thanasilp, and Z. Holmes, Efficient quantum-enhanced classical simulation for patches of quantum landscapes, arXiv preprint arXiv:2411.19896 [10.48550/arXiv.2411.19896](https://doi.org/10.48550/arXiv.2411.19896) (2024).
  - [13] C. Cirstoiu, A fourier analysis framework for approximate classical simulations of quantum circuits, arXiv preprint arXiv:2410.13856 [10.48550/arXiv.2410.13856](https://doi.org/10.48550/arXiv.2410.13856) (2024).
  - [14] A. Angrisani, A. A. Mele, M. S. Rudolph, M. Cerezo, and Z. Holmes, Simulating quantum circuits with arbitrary local noise using pauli propagation, arXiv preprint arXiv:2501.13101 [10.48550/arXiv.2501.13101](https://doi.org/10.48550/arXiv.2501.13101) (2025).
  - [15] B. Fuller, M. C. Tran, D. Lykov, C. Johnson, M. Rossmannek, K. X. Wei, A. He, Y. Kim, D. Vu, K. Sharma, *et al.*, Improved quantum computation using operator backpropagation, arXiv preprint arXiv:2502.01897 <https://doi.org/10.48550/arXiv.2502.01897> (2025).
  - [16] J. Yu, J. R. Moreno, J. T. Iosue, L. Bertels, D. Claudino, B. Fuller, P. Groszkowski, T. S. Humble, P. Jurcevic, W. Kirby, *et al.*, Quantum-centric algorithm for sample-based krylov diagonalization, arXiv preprint arXiv:2501.09702 (2025).
  - [17] K. Yeter-Aydeniz, R. C. Pooser, and G. Siopsis, Practical quantum computation of chemical and nuclear energy levels using quantum imaginary time evolution and Lanczos algorithms, *npj Quantum Information* **6**, 63 (2020).
  - [18] K. Yeter-Aydeniz, B. T. Gard, J. Jakowski, S. Majumder, G. S. Barron, G. Siopsis, T. S. Humble, and R. C. Pooser, Benchmarking quantum chemistry computations with variational, imaginary time evolution, and krylov space solver algorithms, *Advanced Quantum Technologies* **4**, 2100012 (2021).
  - [19] R. LaRose, A. Tikku, É. O’Neel-Judy, L. Cincio, and P. J. Coles, Variational quantum state diagonalization, *npj Quantum Information* **5**, 1 (2019).
  - [20] R. M. Parrish, E. G. Hohenstein, P. L. McMahon, and T. J. Martínez, Quantum computation of electronic transitions using a variational quantum eigensolver, *Physical review letters* **122**, 230401 (2019).
  - [21] N. H. Stair, R. Huang, and F. A. Evangelista, A multireference quantum krylov algorithm for strongly correlated electrons, *Journal of chemical theory and computation* **16**, 2236 (2020).
  - [22] C. Kokail, C. Maier, R. van Bijnen, T. Brydges, M. K. Joshi, P. Jurcevic, C. A. Muschik, P. Silvi, R. Blatt, C. F. Roos, *et al.*, Self-verifying variational quantum simulation of lattice models, *Nature* **569**, 355 (2019).
  - [23] F. Arute, K. Arya, R. Babbush, D. Bacon, J. C. Bardin, R. Barends, S. Boixo, M. Broughton, B. B. Buckley, *et al.*, Hartree-fock on a superconducting qubit quantum computer, *Science* **369**, 1084 (2020).
  - [24] L. Xiaoyue, M. Robbati, A. Pasquale, E. Pedicillo, A. Wright, S. Carrazza, and M. Gluza, Strategies for optimizing double-bracket quantum algorithms, arXiv preprint arXiv:2408.07431 (2024).
  - [25] M. Cerezo, A. Arrasmith, R. Babbush, S. C. Benjamin, S. Endo, K. Fujii, J. R. McClean, K. Mitarai, X. Yuan, L. Cincio, *et al.*, Variational quantum algorithms, *Nature*



- Reviews Physics **3**, 625 (2021).
- [26] M. A. Nielsen and I. L. Chuang, *Quantum Computation and Quantum Information* (Cambridge University Press, Cambridge, 2000).
  - [27] K. Temme, T. J. Osborne, K. G. Vollbrecht, D. Poulin, and F. Verstraete, Quantum metropolis sampling, *Nature* **471**, 87 (2011).
  - [28] A. Y. Kitaev, Quantum measurements and the abelian stabilizer problem, arXiv preprint quant-ph/9511026 (1995).
  - [29] G. Brassard, P. Hoyer, M. Mosca, and A. Tapp, Quantum amplitude amplification and estimation, *Contemporary Mathematics* **305**, 53 (2002).
  - [30] K. C. Tan, D. Bowmick, and P. Sengupta, Quantum stochastic series expansion methods (2020), arXiv:2010.00949.
  - [31] G. H. Low and I. L. Chuang, Hamiltonian simulation by qubitization, *Quantum* **3**, 163 (2019).
  - [32] A. Gilyén, Y. Su, G. H. Low, and N. Wiebe, Quantum singular value transformation and beyond: exponential improvements for quantum matrix arithmetics, in *Proceedings of the 51st Annual ACM SIGACT Symposium on Theory of Computing* (2019) pp. 193–204.
  - [33] Y. Ge, J. Tura, and J. I. Cirac, Faster ground state preparation and high-precision ground energy estimation with fewer qubits, *Journal of Mathematical Physics* **60**, 022202 (2019).
  - [34] M. Motta, C. Sun, A. T. Tan, M. J. O’Rourke, E. Ye, A. J. Minnich, F. G. Brandao, and G. K.-L. Chan, Determining eigenstates and thermal states on a quantum computer using quantum imaginary time evolution, *Nature Physics* **16**, 205 (2020).
  - [35] D. Motlagh, M. S. Zini, J. M. Arrazola, and N. Wiebe, Ground state preparation via dynamical cooling, arXiv preprint arXiv:2404.05810 <https://doi.org/10.48550/arXiv.2404.05810> (2024).
  - [36] M. Gluza, J. Son, B. H. Tiang, Y. Suzuki, Z. Holmes, and N. H. Ng, Double-bracket quantum algorithms for quantum imaginary-time evolution, arXiv preprint arXiv:2412.04554 <https://doi.org/10.48550/arXiv.2412.04554> (2024).
  - [37] S. Lee, J. Lee, H. Zhai, Y. Tong, A. M. Dalzell, A. Kumar, P. Helms, J. Gray, Z.-H. Cui, W. Liu, *et al.*, Evaluating the evidence for exponential quantum advantage in ground-state quantum chemistry, *Nature Communications* **14**, 1952 (2023).
  - [38] Z. Zimborás, B. Koczor, Z. Holmes, E.-M. Borrelli, A. Gilyén, H.-Y. Huang, Z. Cai, A. Acín, L. Aolita, L. Banchi, *et al.*, Myths around quantum computation before full fault tolerance: What no-go theorems rule out and what they don’t, arXiv preprint arXiv:2501.05694 <https://doi.org/10.48550/arXiv.2501.05694> (2025).
  - [39] A. Miller, Z. Zimborás, S. Knecht, S. Maniscalco, and G. García-Pérez, Bonsai algorithm: Grow your own fermion-to-qubit mappings, *PRX Quantum* **4**, 030314 (2023).
  - [40] A. Miller, A. Glos, and Z. Zimborás, Treespilation: Architecture and state-optimised fermion-to-qubit mappings, arXiv preprint arXiv:2403.03992 (2024).
  - [41] Z. Jiang, A. Kalev, W. Mruczkiewicz, and H. Neven, Optimal fermion-to-qubit mapping via ternary trees with applications to reduced quantum states learning, *Quantum* **4**, 276 (2020).
  - [42] P. Jordan and E. Wigner, Über das Paulische Äquivalenzverbot, *Zeitschrift für Physik* **47**, 631 (1928).
  - [43] S. B. Bravyi and A. Y. Kitaev, Fermionic quantum computation, *Annals of Physics* **298**, 210 (2002).
  - [44] M. Chiew and S. Strelchuk, Discovering optimal fermion-qubit mappings through algorithmic enumeration, *Quantum* **7**, 1145 (2023).
  - [45] R. W. Chien and J. Klassen, Optimizing fermionic encodings for both hamiltonian and hardware, arXiv preprint arXiv:2210.05652 (2022).
  - [46] J. R. McClean, M. E. Kimchi-Schwartz, J. Carter, and W. A. De Jong, Hybrid quantum-classical hierarchy for mitigation of decoherence and determination of excited states, *Physical Review A* **95**, 042308 (2017).
  - [47] D. Stilck França and R. Garcia-Patron, Limitations of optimization algorithms on noisy quantum devices, *Nature Physics* **17**, 1221 (2021).
  - [48] E. R. Anschuetz and B. T. Kiani, Beyond barren plateaus: Quantum variational algorithms are swamped with traps, *Nature Communications* **13**, 7760 (2022).
  - [49] M. Larocca and V. Havlicek, Quantum algorithms for representation-theoretic multiplicities, arXiv preprint arXiv:2407.17649 (2024).
  - [50] M. Cerezo, M. Larocca, D. García-Martín, N. L. Diaz, P. Braccia, E. Fontana, M. S. Rudolph, P. Bermejo, A. Ijaz, S. Thanasilp, *et al.*, Does provable absence of barren plateaus imply classical simulability? Or, why we need to rethink variational quantum computing, arXiv preprint arXiv:2312.09121 (2023).
  - [51] H. R. Grimsley, S. E. Economou, E. Barnes, and N. J. Mayhall, An adaptive variational algorithm for exact molecular simulations on a quantum computer, *Nature Communications* **10**, 1 (2019).
  - [52] P. Bermejo, P. Braccia, M. S. Rudolph, Z. Holmes, L. Cincio, and M. Cerezo, Quantum convolutional neural networks are (effectively) classically simulable, arXiv preprint arXiv:2408.12739 (2024).
  - [53] H. L. Tang, V. Shkolnikov, G. S. Barron, H. R. Grimsley, N. J. Mayhall, E. Barnes, and S. E. Economou, Qubit-adapt-vqe: An adaptive algorithm for constructing hardware-efficient ansätze on a quantum processor, *PRX Quantum* **2**, 020310 (2021).
  - [54] H. R. Grimsley, G. S. Barron, E. Barnes, S. E. Economou, and N. J. Mayhall, Adaptive, problem-tailored variational quantum eigensolver mitigates rough parameter landscapes and barren plateaus, *npj Quantum Information* **9**, 10.1038/s41534-023-00681-0 (2023).
  - [55] P. G. Anastasiou, Y. Chen, N. J. Mayhall, E. Barnes, and S. E. Economou, Tetris-adapt-vqe: An adaptive algorithm that yields shallower, denser circuit ansätze, *Physical Review Research* **6**, 10.1103/physrevresearch.6.013254 (2024).
  - [56] M. Ramôa, P. G. Anastasiou, L. P. Santos, N. J. Mayhall, E. Barnes, and S. E. Economou, Reducing the resources required by adapt-vqe using coupled exchange operators and improved subroutines (2024), arXiv:2407.08696 [quant-ph].
  - [57] T. T. Inc., Clinical studies overview – TLD-1433 (Ruvidar™) (2024), accessed: 2024-02-27.
  - [58] E.-J. Kuo, B. Ware, P. Lunts, M. Hafezi, and C. D. White, Energy diffusion in weakly interacting chains with fermionic dissipation assisted operator evolution, *Physical Review B* **110**, 075149 (2024).

- [59] J. W. Mullinax and N. M. Tubman, Large-scale sparse wavefunction circuit simulator for applications with the variational quantum eigensolver, arXiv preprint arXiv:2301.05726 (2023).
- [60] J. W. Mullinax, P. G. Anastasiou, J. Larson, S. E. Economou, and N. M. Tubman, Classical pre-optimization approach for adapt-vqe: Maximizing the potential of high-performance computing resources to improve quantum simulation of chemical applications, arXiv preprint arXiv:2411.07920 (2024).
- [61] O. Reardon-Smith, M. Oszmaniec, and K. Korzekwa, Improved simulation of quantum circuits dominated by free fermionic operations, *Quantum* **8**, 1549 (2024).
- [62] A. Mocherla, L. Lao, and D. E. Browne, Extending matchgate simulation methods to universal quantum circuits, arXiv preprint arXiv:2302.02654 (2023).
- [63] R. D. Somma, Quantum computation, complexity, and many-body physics, arXiv preprint quant-ph/0512209 (2005).
- [64] R. Somma, H. Barnum, G. Ortiz, and E. Knill, Efficient solvability of Hamiltonians and limits on the power of some quantum computational models, *Physical Review Letters* **97**, 190501 (2006).
- [65] V. Galitski, Quantum-to-classical correspondence and hubbard-stratonovich dynamical systems: A lie-algebraic approach, *Phys. Rev. A* **84**, 012118 (2011).
- [66] M. L. Goh, M. Larocca, L. Cincio, M. Cerezo, and F. Sauvage, Lie-algebraic classical simulations for variational quantum computing, arXiv preprint arXiv:2308.01432 (2023).
- [67] E. R. Anschuetz, A. Bauer, B. T. Kiani, and S. Lloyd, Efficient classical algorithms for simulating symmetric quantum systems, *Quantum* **7**, 1189 (2023).
- [68] V. Bettaque and B. Swingle, The structure of the majorana clifford group, arXiv preprint arXiv:2407.11319 (2024).

## Appendix A: Preliminaries

### 1. Introduction to fermionic systems

An  $N$ -mode Fermionic system in second quantization can be described in terms of  $N$  creation operators  $\{a_i^\dagger\}_{i=1}^N$  and annihilation operators  $\{a_i\}_{i=1}^N$  that satisfy the canonical anticommutation relations:

$$\{a_i, a_j\} = \{a_i^\dagger, a_j^\dagger\} = 0, \quad \{a_i^\dagger, a_j\} = \delta_{ij}. \quad (\text{A1})$$

Mathematically, the  $N$ -mode Fermionic system is equivalent to the  $N$ -dimensional Fock space  $\mathcal{F}(\mathbb{C}^N)$ , a  $2^N$ -dimensional Hilbert space spanned by the so-called Fock basis. The operators defined above allow us to define the basis as follows. First, the Fermionic vacuum  $|\text{vac}_f\rangle$  is defined to be the unique vector such that  $a_j |\text{vac}_f\rangle = 0$  for all  $j = 1, \dots, N$ . The remaining basis elements, namely *Fock* states, can be constructed by considering all possible combinations of occupation numbers  $n_j \in \{0, 1\}$ :

$$|n_1 n_2 \dots n_N\rangle := \prod_{j=1}^N (a_j^\dagger)^{n_j} |\text{vac}_f\rangle. \quad (\text{A2})$$

Creation and annihilation operators are not the only operators that can define the Fermionic space. It is also common to define an equivalent set of so-called Majorana operators  $\{m_k\}_{k=1}^{2N}$  as

$$m_{2j-1} := a_j^\dagger + a_j, \quad (\text{A3})$$

$$m_{2j} := i(a_j^\dagger - a_j). \quad (\text{A4})$$

Such operators obey many useful properties, such as being unitary and self-adjoint, obeying relations

$$m_i^\dagger = m_i, \quad \{m_i, m_j\} = 2\delta_{ij}. \quad (\text{A5})$$

These operators play an analogous role in the Fermionic Clifford group as Pauli operators do in the qubit Clifford group. For a comprehensive introduction to the structure of the Majorana Clifford group see Ref. [68].

The above ways of defining Fermionic systems allow us to provide two equivalent forms of an  $N$ -mode second-quantized Fermionic Hamiltonian:

$$\begin{aligned} \mathcal{H}_f &= \sum_{ij} h_{ij} a_i^\dagger a_j + \sum_{ijkl} h_{ijkl} a_i^\dagger a_j^\dagger a_k a_l \\ &= \sum_{ij} i c_{ij} m_i m_j + \sum_{ijkl} c_{ijkl} m_i m_j m_k m_l. \end{aligned} \quad (\text{A6})$$

for coefficients  $h_{ij}$ ,  $h_{ijkl}$ ,  $c_{ij}$  and  $c_{ijkl}$ . The equivalence between these forms comes directly from the linear dependency presented in Eq. (A3).

Any Fermionic operator can be uniquely expressed as a linear combination of Majorana monomials. Hence, up to a sign, each unique product of Majorana operators can be associated with a  $2N$ -dimensional binary vector  $\mathbf{b} = (b_1, \dots, b_{2N})$ ,  $b_i \in \{0, 1\}$  through the expression

$$M_{\mathbf{b}} = i^{r_{\mathbf{b}}} m_1^{b_1} m_2^{b_2} \dots m_{2N}^{b_{2N}}. \quad (\text{A7})$$

We define the length of a Majorana monomial as the 1-norm of vector  $\mathbf{b}$ ,  $\|\mathbf{b}\|_1 = \sum_{i=1}^{2N} b_i$ . Let us relabel a Majorana monomial of length  $w$  as  $m_{x_1} \dots m_{x_w}$ . All monomials referenced throughout this document have been made Hermitian by multiplying the anti-Hermitian ones by the imaginary unit  $i$ . Concretely,

$$(m_{x_1} \dots m_{x_w})^\dagger = m_{x_w} \dots m_{x_1} = (-1)^{\sum_{j=1}^{w-1} w-j} m_{x_1} \dots m_{x_w} = (-1)^{w(w-1)/2} m_{x_1} \dots m_{x_w} \quad (\text{A8})$$

Thus if  $w$  or  $w - 1$  is a multiple of 4 then  $m_{x_1} \dots m_{x_w}$  is already Hermitian and  $r = 0$ , but otherwise  $m_{x_1} \dots m_{x_w}$  is antihermitian and  $r = 1$  so that the factor of  $i$  makes the monomial Hermitian.

Notice that, owing to the anti-commutation relations between Majorana operators, any repeated terms in a monomial cancel out, so each operator can appear at most once in a monomial. Also, any monomial is equal to itself upon reshuffling of its elements up to a sign, so we will assume  $x_1 < x_2 < \dots < x_w$  throughout without loss of generality.

## 2. Algorithm overview

We are interested in computing

$$f(\boldsymbol{\theta}) := \langle H \rangle_{\boldsymbol{\theta}} = \text{Tr} [U(\boldsymbol{\theta}) \varrho U(\boldsymbol{\theta})^\dagger H] \quad (\text{A9})$$

where  $\varrho = |n_1 n_2 \dots n_N\rangle\langle n_1 n_2 \dots n_N|$ , with  $n_i \in \{0, 1\}$ , is a Fock basis state. The circuit

$$U(\boldsymbol{\theta}) = \prod_{j=1}^L e^{-i\theta_j M_{\mathbf{b}_j}/2} \quad (\text{A10})$$

consists of a sequence of  $L$  Fermionic gates where each gate is generated by a Hermitian Fermionic generator  $M_{\mathbf{b}_j}$  which is a  $w$ -monomial. We will assume  $w$  even and  $w \leq k$  for all gates and for some pre-defined value of  $k$  (typically  $k = 4$ ). We will assume that the observable  $H$  is composed of a sum of polynomially many  $w$ -monomials. That is,  $H = \sum_{\mathbf{b}} \alpha_{\mathbf{b}} M_{\mathbf{b}}$  where the  $M_{\mathbf{b}}$  are  $w$ -monomials with  $w \leq k'$ . Typically,  $k' = 4$ , for interacting Hamiltonians.

Our Majorana Propagation method, analogously to Pauli propagation algorithms, works in the Heisenberg picture where the initial operator (here the observable  $H$ ) is often sparse in the Majorana basis. In this basis, the operator is back-propagated through the circuit, i.e., we compute  $U(\boldsymbol{\theta})^\dagger H U(\boldsymbol{\theta})$ , and finally overlap with the initial state  $\varrho$ . It is well known that the effect of applying a unitary gate generated by a single Pauli string  $P$  to another Pauli string  $Q$  is given by,

$$e^{i\theta P/2} Q e^{-i\theta P/2} = \begin{cases} Q, & [P, Q] = 0, \\ \cos(\theta)Q + i \sin(\theta)PQ, & \{P, Q\} = 0. \end{cases} \quad (\text{A11})$$

We recall that the standard textbook derivation of Eq. (A11) can be computed by Taylor-expanding  $e^{i\theta P/2}$  and using  $P^2 = I$ . For Majorana monomials we similarly have  $M^2 = I$ , and thus the analogous expression holds here. Namely, we have

$$e^{i\theta M'/2} M e^{-i\theta M'/2} = \begin{cases} M, & [M', M] = 0, \\ \cos(\theta)M + i \sin(\theta)M'M, & \{M', M\} = 0. \end{cases} \quad (\text{A12})$$

The Heisenberg evolved operator,  $U(\boldsymbol{\theta})^\dagger H U(\boldsymbol{\theta})$ , can be computed by applying each gate to each of the monomials in the observable in turn using Eq. (A12). The final expectation function takes the form

$$f(\boldsymbol{\theta}) = \sum_j c_{\mathbf{b}}(\boldsymbol{\theta}) \text{Tr}[\varrho M_{\mathbf{b}}], \quad (\text{A13})$$

where  $c_{\mathbf{b}}(\boldsymbol{\theta})$  are the coefficients of the back-propagated Majorana operators  $M_{\mathbf{b}}$ . These coefficients capture both the initial length of each of the relevant monomial in the target observable  $H$  and the sine and cosine coefficients that have been picked up during the propagation.

## Appendix B: Coefficient and small angle truncations

Here we suppose that we are interested in simulating a small angle subregion of the surrogate landscape. Let us then define

$$\mathcal{V}_L(r) := \{\boldsymbol{\theta}; \forall i \theta_i \in [-r, r]\}, \quad (\text{B1})$$

as the hypercube of parameter space centred around the point  $\mathbf{0}$ , and

$$\mathcal{D}_L(r) := \text{Unif}[\mathcal{V}_L(r)] \quad (\text{B2})$$

as a uniform distribution over the hypercube  $\mathcal{V}_L(r)$ . It can be shown that for any randomly chosen  $\boldsymbol{\theta} \sim \mathcal{D}_L(r)$  the error induced by the small angle truncation strategy can be kept small. Combining this with the observation that small angle truncation keeps the number of paths tractable, one obtains the following guarantee on the efficiency of small angle truncation Majorana Propagation.

**Proposition 1** (Time complexity of small-angle Majorana Propagation). *Consider an expectation function  $f(\theta) = \text{Tr}[U(\theta)\varrho U(\theta)^\dagger H]$  with  $\varrho$  the initial state, an observable  $H = \sum_{\mathbf{b}} a_{\mathbf{b}} M_{\mathbf{b}}$ , where at most  $N \in \mathcal{O}(\text{poly}(n))$  coefficients  $a_j$  are non zero, with  $\|\mathbf{a}\|_1 \in \mathcal{O}(1)$ , and a parametrized circuit of the form of Eq. (A10). If the expectation values  $\text{Tr}[\varrho M_{\mathbf{b}}]$  of the initial state  $\varrho$  with any Majorana operator  $M_{\mathbf{b}}$  can be efficiently computed, then a runtime of*

$$t \in \mathcal{O}\left(N \cdot L^{\log\left(\frac{1}{\epsilon^{2\delta}}\right)}\right), \quad (\text{B3})$$

*suffices to classically simulate  $f(\theta)$  up to an error  $\epsilon$  with probability at least  $1 - \delta$  for random  $\theta \sim \mathcal{D}_L(r)$  with*

$$r \in \mathcal{O}\left(\frac{1}{\sqrt{L}}\right). \quad (\text{B4})$$

*Similarly, with a runtime of*

$$t \in \mathcal{O}\left(N \cdot L^{\log\left(\frac{1}{\epsilon}\right)}\right) \quad (\text{B5})$$

*we can classically simulate  $f(\theta)$  up to an error  $\epsilon$  for all  $\theta$  in the hypercube  $\mathcal{V}_L(r)$  with*

$$r \in \mathcal{O}\left(\frac{1}{L}\right). \quad (\text{B6})$$

*Proof.* The proof follows from substituting Eq. (A12) and  $|\text{Tr}[\varrho M_{\mathbf{b}}]| \leq 1$  into the proof of Theorem 3 in Ref. [12].  $\square$

### Appendix C: Length Truncation

In the previous section we detailed coefficient and small-angle truncation strategies which cut terms from the sum in Eq. (A13) where the prefactor  $c_{\mathbf{b}}(\theta)$  that are either small or, in the case of the latter, likely to be small. Here we detail an alternative truncation strategy that aims to cut terms from the sum in Eq. (A13) where  $\text{Tr}[\varrho M_{\mathbf{b}}]$  is likely small.

The core intuition here is that in order for a term  $\text{Tr}[\varrho M_{\mathbf{b}}]$ , where  $\varrho$  is a Fock state, to be non-zero all the Majorana operators in the monomial  $M_{\mathbf{b}}$  are paired. That is,  $\text{Tr}[\varrho M_{\mathbf{b}}] = 0$  if and only if for every even Majorana operator  $m_{2i}$  in the monomial  $M_{\mathbf{b}}$ , the Majorana operator  $m_{2i+1}$  is also in the monomial  $M_{\mathbf{b}}$  (this can be seen immediately from the definition of the Majorana operator). Next we observe that in general the higher the length  $w$  of the Majorana monomial (for  $w < N$ ) the lower the probability that the monomial is paired.

This motivates a *length truncation* strategy. At each step, after each gate is applied, all terms corresponding to Majorana monomials with length above a certain threshold are to be discarded. In typical circuits, the method is expected to result in an accurate computation since high-length monomials truncated along the way would most likely keep increasing in length along the way, therefore sharply decreasing their relative importance for the quantity under evaluation. This idea is analyzed with a greater level of detail and precision in the next two subsections.

#### 1. The contribution of typical high length Majorana monomials are exponentially suppressed

In this subsection we substantiate the claim that the higher length Majorana monomials  $M_{\mathbf{b}}$ , that arise during a propagation, are more likely to annihilate when we compute their overlap with the initial Fock state. Intuitively, this can be seen by supposing that, due to the circuit's complexity, all high-length  $w$ -monomials carry a similar length. There are  $\binom{2N}{w}$  such monomials. The number of these that are paired is  $\binom{N}{w/2}$ . The probability  $P(w)$  that any randomly chosen length  $w$  Monomial  $M_{\mathbf{b}}$  is paired (and therefore  $\text{Tr}[\varrho M_{\mathbf{b}}] \neq 0$ ) is given by

$$P(w) = \frac{\binom{N}{w/2}}{\binom{2N}{w}}. \quad (\text{C1})$$

Figure 2 depicts the pairing probability as a function of  $w$  for  $N = 100$ . It is visually clear that only  $w \approx 0$  and  $w \approx 2N$  contribute significantly, all other terms contributing many orders of magnitude less. This observation is formalized by the following theorem where we show that the contribution of any random chosen Monomial with both  $w \in \Theta(N)$  and  $(2N - w) \in \Theta(N)$  is exponentially in  $N$  suppressed. Conversely, the contribution of terms with  $w \in \mathcal{O}(1)$  are only polynomially suppressed.

**Theorem 1** (The contribution of high length Majoranas are exponentially suppressed). *The probability  $P(w)$  that any randomly chosen  $N$ -mode Majorana monomial with length  $w$ , where both  $w \in \Theta(N)$  and  $(2N - w) \in \Theta(N)$ , has a non-zero expectation in any given Fock state is exponentially suppressed in  $N$ , that is*

$$P(w) \in \mathcal{O}(r^{-N}) \quad (\text{C2})$$

where  $r > 1$ . Furthermore, the minimal probability is obtained for  $w = N$  with

$$\min_w P(w) = P(N) \in \mathcal{O}(2^{-N}). \quad (\text{C3})$$

Conversely, if  $w \in \mathcal{O}(1)$  we have that

$$P(w) \in \Omega\left(\frac{1}{\text{poly}(N)}\right). \quad (\text{C4})$$

*Proof.* As argued above, only paired Majorana modes have a non-vanishing expectation in any Fock state and this occurs with the probability  $P(w)$  stated in Eq. (C1). We will start by showing that for  $w = cN$

$$P(w) \in \mathcal{O}(r^{-N}) \quad (\text{C5})$$

for some  $r > 1$ . To do so we employ the following inequality

$$\left(\frac{m}{k}\right)^k \leq \binom{m}{k} \leq \left(\frac{em}{k}\right)^k, \quad (\text{C6})$$

to obtain

$$P(w) \leq \left(\frac{ew}{2N}\right)^{w/2}. \quad (\text{C7})$$

Thus if we set  $w/2 = cN$  ( $0 < c < 1$ ) we have that

$$P(w) \leq p^{cN} \quad (\text{C8})$$

where  $p = ec$ . Hence if  $c < 1/e$ , corresponding to  $w < 2N/e < 0.74N$ , we have that  $0 < p < 1$  and thus  $P(w) = r^{-N}$  with  $r = p^{-c} > 1$ . To quantify the scaling of  $P(w)$  in the region  $0.74N \leq w \leq N$  we note that  $P(w)$  decreases monotonically with  $w$  to its minimal value at  $P(N)$  and hence

$$P(w) \leq r^{-N} \quad (\text{C9})$$

with  $r = p^{-c}$  for some  $0 < p < 1$  for any  $w = Nc$ ,  $0 < c < 1$ . Finally, since  $P(w)$  is symmetric with respect to  $w = N$ ,  $P(w) = P(2N - w)$ , the result applies to any  $w = 2Nc$ , as claimed.

To bound the minimal value of  $P(w)$  at  $w = N$  we can use the following Binomial coefficient bound

$$\frac{4^N}{\sqrt{\pi(N + 1/3)}} \leq \binom{2N}{N} \leq \frac{4^N}{\sqrt{\pi(N + 1/4)}}. \quad (\text{C10})$$

Thus we can upper bound the minimal value of  $P(w)$  as

$$\min_w P(w) = P(N) \leq 4^{-N/2} \sqrt{\frac{N + 1/3}{N/2 + 1/4}} \leq 4^{-N/2} \sqrt{\frac{3N}{N}} \in \mathcal{O}(2^{-N}). \quad (\text{C11})$$

Finally, we can find a lower bound  $P(w)$  for  $w \in \mathcal{O}(1)$  using Eq. (C6) to give

$$P(w) \geq \left(\frac{2N}{w}\right)^{w/2} \left(\frac{e2N}{w}\right)^{-w} = \left(\frac{2N}{w}\right)^{-w/2} e^{-w} = \left(\frac{w}{2e^2N}\right)^{w/2} \geq \left(\frac{w}{15N}\right)^{w/2}. \quad (\text{C12})$$

Thus if  $w \in \mathcal{O}(1)$  we have that  $P(w) \in \Omega\left(\frac{1}{\text{poly}(N)}\right)$ . □



## 2. The probability of backflow is suppressed

In the previous subsection we saw that only very low or very high length monomials contribute substantially to Fock state expectation values. Two points must now be addressed:

1. The fact that it is safe to disregard high-length  $w$ -monomials in the final observable does not imply that it is safe to disregard high-length  $w$ -monomials at intermediate steps; high-length  $w$ -monomials at step  $T$  may still evolve towards low-length terms in  $O_D$ , so their removal at step  $T$  may result in large errors.
2. High-length terms could evolve towards  $w = 2N$ , where their contribution matters, so truncating high-length elements early in the simulation may result in large errors.

As we shall now see, the answer to these concerns is that a typical dynamics leads to operators clustering around  $w = N$ , and the probability for their length to increase all the way to  $w \approx 2N$  or to decrease back to  $w \approx 0$  is negligible.

**Theorem 2** (Suppression of backflow). *Consider the propagation of a length  $w$  Majorana monomial  $M$  under a length  $k$  generator of rotation  $M'$  as per Eq. (A12). We assume that  $[M', M] \neq 0$  such that the propagation causes branching and we denote the length of the new Majorana monomial,  $M'M$ , as  $w'$ . Let  $P_+$  and  $P_-$  denote the probabilities that the propagation increases ( $w' > w$ ) and decreases ( $w < w'$ ) operator length. The following statements hold:*

1. Any rotation under a  $k = 2$  length generator  $M$  leaves the initial length  $w$  unchanged,  $P_+ = P_- = 0$ .
2. Consider a uniformly randomly chosen  $N$ -mode Majorana monomial of length  $w$  and a randomly chosen generator of length  $k = 4$ . The ratio of the probabilities that propagation decreases versus increases operator length is:

$$R := \frac{P_-}{P_+} = \frac{(w-1)(w-2)}{(2N-1-w)(2N-2-w)}. \quad (\text{C13})$$

Thus for any  $w \ll N$  the backflow is suppressed with the suppression quadratic in  $N$  for  $w \in \mathcal{O}(1)$ .

3. For any  $w \in \mathcal{O}(1)$  and  $k \in \mathcal{O}(1)$  with  $2 \leq k \leq w$  such that  $wk < N$  we have that

$$R \in \mathcal{O}(1/N^2). \quad (\text{C14})$$

*Proof. Part 1)* Let us denote the number of overlapping Majorana operators between  $M$  and  $M'$  as  $s$ . The commutator  $[M, M'] \neq 0$ , i.e., the propagation only causes branching, if and only if the number of Majorana operators common to both monomials is odd. Thus in what follows we can assume  $s$  is odd.

Next, since even repetitions of Majorana operators in a monomial cancel out, the length of the monomial appearing in the branching term,  $M'M$ , must be smaller than the sum of each monomial's length. More precisely, the length  $w'$  of the term  $M'M$  is  $w' = k + w - 2s$ . We can thus see that if  $s < k/2$ , the branching process increases Majorana length,  $w' > w$ , while  $w' < w$  if  $s > k/2$  and the length is left unchanged,  $w' = w$  if  $s = k/2$ . We can therefore immediately see that if  $k = 2$  then  $s = k/2 = 1$  and propagation does not increase monomial length (proving the first claim in Theorem 2).

*Part 2)* Next, as before let us consider the ‘random Majorana’ limit where we assume that all Majorana monomials of any given length are equally likely. In this case, the probability that any two randomly chosen Majorana monomials of lengths  $w$  and  $k$  respectively overlap on precisely  $s$  modes is given by

$$P(N, w, k, s) = \frac{\binom{k}{s} \binom{2N-k}{w-s}}{\binom{2N}{w}}. \quad (\text{C15})$$

To see this we can start by assuming that the first Majorana monomial of  $k$  elements is fixed. There is no loss of generality in doing so since we will count the selections for the second string relative to this fixed set. The second majorana monomial is chosen by selecting  $w$  elements out of  $2N$ . Hence, the total number of possible selections is  $\binom{2N}{w}$ . To have exactly  $s$  overlapping elements between the two strings, the following must occur:

1. Choose  $s$  overlapping elements: From the fixed string of  $k$  elements, choose  $s$  elements. This can be done in  $\binom{k}{s}$  ways.

2. Choose the remaining  $w - s$  non-overlapping elements: The remaining  $w - s$  elements of the second string must come from the  $2N - k$  elements that are *not* in the fixed string. This selection can be made in  $\binom{2N-k}{w-s}$  ways.

Thus, the total number of favorable outcomes is:

$$\binom{k}{s} \binom{2N-k}{w-s}. \quad (\text{C16})$$

The probability that the two strings overlap in exactly  $s$  elements is the ratio of the number of favorable outcomes to the total number of outcomes:

$$P(N, w, k, s) = \frac{\binom{k}{s} \binom{2N-k}{w-s}}{\binom{2N}{w}}. \quad (\text{C17})$$

This proves Eq. (C15).

Next, we focus on the commonly encountered scenario where  $k = 4$ . In this case, we can compute an exact compact expression for the ratio between the probability that any branching event decreases Majorana length as compared to increases it. Namely, as if  $s < k/2$ , the branching process increases Majorana length and decreases it if  $s > k/2$ , in this case this ratio is given by

$$R := \frac{P_-}{P_+} = \frac{P(N, w, 4, 3)}{P(N, w, 4, 1)}. \quad (\text{C18})$$

If we substitute Eq. (C15) into  $R$  we find that

$$R = \frac{P(N, w, 4, 3)}{P(N, w, 4, 1)} = \frac{\binom{4}{3} \binom{2N-4}{w-3}}{\binom{4}{1} \binom{2N-4}{w-1}} = \frac{\binom{2N-4}{w-3}}{\binom{2N-4}{w-1}}, \quad (\text{C19})$$

where we use that as binomial coefficients are symmetric we have  $\binom{4}{3} = \binom{4}{1}$ . Using the explicit expression for the binomial coefficients this simplifies to

$$R = \frac{(w-1)!(2N-3-w)!}{(w-3)!(2N-1-w)!} = \frac{(w-1)(w-2)}{(2N-1-w)(2N-2-w)}. \quad (\text{C20})$$

Thus for  $w \in \mathcal{O}(1)$  we see that  $R$  is quadratically suppressed in  $N$ .

*Part 3)* A similar suppression is obtained whenever  $k$  and  $w$  are much smaller than  $2N$ . In this case we have that the probability that the length decreases is the sum of  $P(N, k, w, s)$  for all odd values of  $s$  greater than  $k/2$  (up to a maximum value of  $k$ ),

$$P_- = \sum_{k/2 < 2j+1 < k} P(N, w, k, 2j+1). \quad (\text{C21})$$

Similarly, the probability that the length increases is the sum of  $P(N, k, w, s)$  for all odd values of  $s$  less than  $k/2$ , i.e.,

$$P_+ = \sum_{0 < 2j+1 < k/2} P(N, w, k, 2j+1). \quad (\text{C22})$$

There are the same number of terms in the sums in Eq. (C21) and Eq. (C22) and so we can bound  $R$  as

$$R \leq \frac{P_{\max}}{P_{\min}} \quad (\text{C23})$$

where

$$\begin{aligned} P_{\max} &:= \max_{j \in \mathbb{Z}^+} \{P(N, w, k, 2j+1)\}_{k/2 < 2j+1 < k} \\ P_{\min} &:= \min_{j \in \mathbb{Z}^+} \{P(N, w, k, 2j+1)\}_{0 < 2j+1 < k/2}. \end{aligned} \quad (\text{C24})$$

In the limit that  $2N$  is much greater than  $w$  and  $k$  (and  $w \geq k$ ) the probability  $P(N, k, w, s)$  decreases monotonically in  $s$ . This can be seen by noting that in this limit the ratio of  $P(N, k, w, s+1)$  and  $P(N, k, w, s)$  is less than 1 for all values of  $0 < s < k$ . Namely, using the identities

$$\frac{\binom{k}{s+1}}{\binom{k}{s}} = \frac{k-s}{s+1} \quad \text{and} \quad \frac{\binom{2N-k}{w-s-1}}{\binom{2N-k}{w-s}} = \frac{w-s}{2N-k-w+s+1}, \quad (\text{C25})$$

we have:

$$\frac{P(N, k, w, s+1)}{P(N, k, w, s)} = \frac{(k-s)(w-s)}{(s+1)(2N-k-w+s+1)} \quad (\text{C26})$$

which is clearly less than 1 for all  $0 < s < k$  in the limit that  $w$  and  $k$  are much less than  $N$ .

More precisely, Eq. (C26) is less than 1 (and  $P(N, k, w, s)$  decreases monotonically in  $s$ ) in the limit that  $wk < N$  (for  $k \geq 2$  and  $w \geq 2$ ). To see this we first note that Eq. (C26) takes the maximal value when  $s = 0$ . This can be seen by taking the log of Eq. (C26) to give

$$F(s) := \ln(k-s) + \ln(w-s) - \ln(s+1) - \ln(2N-k-w+s+1). \quad (\text{C27})$$

Differentiating with respect to  $s$  then yields

$$F'(s) = -\frac{1}{k-s} - \frac{1}{w-s} - \frac{1}{s+1} - \frac{1}{2N-k-w+s+1}. \quad (\text{C28})$$

We can assume that  $s < k$  (if  $s = k$  then the ratio in Eq. (C26) evaluates to 0 and so is less than 1 as required) and  $s < w$  (as we already assumed  $k \leq w$ ). We now further assume that  $2N-k-w+s+1 > 0$  for all  $s$ , which holds if

$$w+k < 2N+1. \quad (\text{C29})$$

Thus each of the denominators in Eq. (C28) are positive, making each term negative. Thus,  $F'(s) < 0$  and so the ratio in Eq. (C26) is strictly decreasing in  $s$ . Because  $R(s)$  is strictly decreasing, its maximum is attained when  $s$  is smallest (assuming  $s \geq 0$ ), i.e., at  $s = 0$ . We then require that

$$\frac{kw}{2N-k-w+1} < 1. \quad (\text{C30})$$

This holds if

$$kw + k + w < 2N + 1. \quad (\text{C31})$$

A looser but more compact bound can be obtained by noting that for  $k \geq 2$  and  $w \geq 2$  we have  $k+w \leq kw$  and so the bound in Eq. (C31) holds if

$$wk < N. \quad (\text{C32})$$

We have thus established that  $P(N, k, w, s)$  is monotonically decreasing if  $wk < N$ .

Returning to our original goal of bounding the ratio of forwards and backflow via Eq. (C24), we can use the fact that  $P(N, k, w, s)$  is monotonically decreasing to conclude that

$$P_{\max} = P(N, w, k, s_{\max}) \quad (\text{C33})$$

$$P_{\min} = P(N, w, k, s_{\min}) \quad (\text{C34})$$

where  $s_{\max}$  ( $s_{\min}$ ) is the odd number that is closest to  $k/2$  while strictly greater than (less than)  $k/2$ . For example, if  $k$  is a multiple of 4, we have  $s_{\max} = k/2 + 1$  and  $s_{\min} = k/2 - 1$ . In complete generality we have that

$$\begin{cases} s_{\max} = k/2 + 1, s_{\min} = k/2 - 1 & k = 4l \\ s_{\max} = k/2 + 1/2, s_{\min} = k/2 - 3/2 & k = 4l + 1 \\ s_{\max} = k/2 + 2, s_{\min} = k/2 - 2 & k = 4l + 2 \\ s_{\max} = k/2 + 3/2, s_{\min} = k/2 - 1/2 & k = 4l + 3, \end{cases} \quad (\text{C35})$$

where  $l$  is some positive integer.

We can use these expressions in Eq. (C23) to bound  $R$ . Namely, for the case where  $k$  is a multiple of 4 we have

$$R \leq \frac{P(N, k, w, k/2 + 1)}{P(N, k, w, k/2 - 1)} = \frac{(w - k/2 + 1)(w - k/2)}{(2N - k/2 - w + 1)(2N - k/2 - w)}. \quad (\text{C36})$$

The ratio can be similarly bounded in each of the other three cases above. The exact expression varies from case to case but in all cases we find a suppression that is at least quadratic in  $N$  for constant  $k$  and  $w$ .  $\square$

## Appendix D: Numerical simulations

In this section, we provide the details about the numerical simulations presented in the main section.

The simulations presented in Table I were run on the Vega supercomputer. MP and Qiskit simulations were run on a single CPU node (dual-socket AMD Rome 7H12, 256GB RAM) using 8 CPU threads. CUDA-Q simulations were run on a single GPU (node architecture: dual-socket AMD Rome 7H12, 512 GB RAM, 4x Nvidia A100, 40GB HBM2). The CUDA-Q MPS simulations were carried out with default parameters and a maximum bond dimension  $\chi = 64$ .

Each simulation is repeated 3 times and the results presented in the table are the average of the 3 runs. For MP, the circuits consist of exponentiations of Majorana monomials. For all the other, the fermionic ansatz was transformed via Jordan-Wigner F2Q mapping, which transforms Majorana monomials exponentiations into Pauli exponentiations. For statevector simulators, the provided circuits were not transpiled. For CUDA-Q MPS, the transpiled input circuits yielded better timings than the untranspiled ones, and were consequently used for the table. The transpilation is performed for all-to-all connectivity, using Steiner-tree based implementation for Fermionic gates from [40] followed by Qiskit transpiler optimization level 1 with the basis gate set of generic single-qubit rotation gate and CNOT. The resulting circuits have 616, 3470 and 13,676 CNOTs, respectively, for 28-, 40- and 52-mode circuits.

The code snippets for obtaining the results are presented below. For Qiskit, the quantum circuit is a `QuantumCircuit` and the Hamiltonian is a `SparsePauliOp` object. For CUDA-Q, the quantum circuit is a `kernel` and the Hamiltonian is a `SpinOperator` object.

### Qiskit SV

```
sv = Statevector.from_instruction(qc)
ev = sv.expectation_value(hamiltonian_qiskit)
```

### CUDA-Q SV

```
cudaq.set_target("nvidia", option="fp64")
energy = estimate_energy_parametrized_kernel(kernel, operator)
```

### CUDA-Q MPS

```
cudaq.set_target("tensornet-mps")
energy = estimate_energy_parametrized_kernel(kernel, operator)
```

## Appendix E: Upper bound to state error

Consider the so-called spectral gap of the Hamiltonian, that is, the difference between its second lowest eigenvalue  $E_1$  and its lowest eigenvalue  $E_0$ . Without loss of generality, let us further assume a given quantum state  $|\psi\rangle$  to have a relative error  $p = \frac{\langle\psi|H|\psi\rangle - E_0}{E_1 - E_0} \leq 1$ . Expressing  $|\psi\rangle$  in the eigenbasis of the Hamiltonian  $|\psi\rangle = \sum_k \alpha_k |E_k\rangle$ , we can define the following bound,

$$\begin{aligned} (E_1 - E_0)p &= \langle\psi|H|\psi\rangle - E_0 = \sum_{k,m} \alpha_k^* \alpha_m E_m \langle E_k|E_m\rangle - E_0 = \sum_k |\alpha_k|^2 E_k - E_0 \\ &\geq (1 - |\alpha_0|^2)E_1 + |\alpha_0|^2 E_0 - E_0 = (E_1 - E_0)(1 - |\alpha_0|^2). \end{aligned} \quad (\text{E1})$$

Assuming a non-degenerate ground state ( $E_1 > E_0$ ), comparing the left-hand side with the right-hand side of Eq. (E1) yields a lower bound for the overlap, namely  $|\alpha| \geq \sqrt{1-p}$  and, consequently, we can define the upper bound to the state error as

$$\text{upper bound to state error} \equiv 1 - |\alpha_0| \leq 1 - \sqrt{1-p}. \quad (\text{E2})$$

Hence, by knowing the relative to spectral gap error of a Hamiltonian, we can compute an upper bound to the overlap error between the obtained state  $|\psi\rangle$  and the target state. For example, in the case of the ground state of TLD1433 with a 52-mode active space, optimizing the quantum circuit to an absolute error of 10 mHa error gives a relative error of  $p \approx 5\%$ , and thus state error 2.53%. We obtain  $E_1$  and  $E_0$  from state-specific DMRG calculations within the various active orbital spaces.